Experimental evidence of liquid feeding during solidification of a steel

Agarwal, G.; Amirthalingam, M.; Moon, S. C.; Dippenaar, R. J.; Richardson, I. M.; Hermans, M. J.M.

DOI
10.1016/j.scriptamat.2017.11.003

Publication date
2018

Document Version
Accepted author manuscript

Published in
Scripta Materialia

Experimental evidence of liquid feeding during solidification of a steel

G. Agarwal[a,*], M. Amirthalingam[b], S.C. Moon[c], R.J. Dippenaar[c], I.M. Richardson[a], M.J.M. Hermans[a]

[a]*Department of Materials Science and Engineering, Faculty of 3mE, Delft University of Technology, Mekelweg 2, 2628CD, Delft, The Netherlands*
[b]*Department of Metallurgical and Materials Engineering, Indian Institute of Technology Madras, Chennai, 600036, India*
[c]*School of Mechanical, Materials and Mechatronic Engineering, Faculty of Engineering and Information Sciences, University of Wollongong, Wollongong, Australia*

Abstract

Sufficient liquid feeding under constrained solidification conditions like, those experienced in welding and casting, is vital to avoid solidification cracking. We present the results of unique in-situ experimental observations of liquid feeding in a solidifying steel melt pool. Liquid feeding was observed in the inter-cellular regions during the terminal stage of solidification. An average liquid flow speed of 450-500 $\mu m\,s^{-1}$ was found. A pressure difference of the order of 10^4 Pa is calculated to cause the liquid flow. The rate of solidification shrinkage and the rate of deformation were found to be less than the rate of liquid feeding.

Keywords: Solidification, Steel, Solidification cracking, Hot tearing, *In-situ*

Some alloys are susceptible to cracking during solidification [1]. Solidification cracking during welding (similar to hot tearing during casting) has been studied for several decades [2, 3, 4, 5, 6]. Presently, it is accepted that a complex interplay between two fundamental factors; solidifying microstructure and restraint, leads to solidification cracking [7]. Upon cooling, a solidifying melt contracts due to both solidification shrinkage and thermal contraction. As the dendritic network becomes coherent, thermal strains are induced. If the remaining liquid is not able to compensate this deformation, cracking occurs. Eskin *et al.* [8] reviewed various hot tearing models for casting, including critical stress, strain and strain rate based criteria that lead to cracking. Nevertheless, a unified model involving the dominant physical factors is still lacking. This is partly due to the fact that solidification cracking occurs close to the solidus temperature (1673 K and above for low carbon steels) involving solid and liquid phases (mushy zone), limiting the scope of direct experimental based investigations. As a result, the various theories and models are rather difficult to verify.

Metallurgical factors that affect the cracking susceptibility include solidification temperature range, dendrite coherency, surface tension of the interdendritic liquid, viscosity, liquid feeding

*Corresponding author
Email address: g.agarwal@tudelft.nl (G. Agarwal)

tendency, grain size and shape, solute segregation in the final stages of solidification *etc*. Liquid feeding is one of the most important factors that helps to avoid solidification cracking and likewise, is included in most of the models [1, 9, 10]. The early work of Feurer [9] was based on rate of feeding and rate of shrinkage effects on hot cracking phenomena. Cracking occurs if during solidification, the rate of feeding of the liquid in the inter-dendritic region is less than the rate of shrinkage of the solid being formed. The model proposed by Rappaz *et al.* [10] considered liquid feeding due to deformation of the coherent dendritic network and shrinkage. If the liquid feeding in the inter-dendritic region of the mushy zone is insufficient to compensate for the shrinkage and cumulative deformation of the mushy zone, the pressure drops below a certain cavitation pressure and voids form, grow and eventually coalesce to form a crack. Recently, Kou [1] proposed a model focussing on similar events occurring at grain boundary level.

Observing the solidification process in the mushy zone in welding conditions is difficult. In the past decade, high energy X-rays sources have facilitated the *in-situ* study of solidification behaviour in many metallic materials [11, 12, 13, 14]. These studies are mostly focussed on Al-Cu, Sn-Pb, Al-Ni and other such systems with relatively low liquidus temperatures [15]. Studies in Fe-C systems are in general focussed on solid state phase transformations. Nagira *et al.* [15] observed *in-situ* deformation in semi-solid carbon steel. They studied the deformation mechanism under direct shear of the steel with a globular morphology and solid fraction between 55-65 %. Several other techniques like directional solidification (Bridgman technique [16]), high speed camera observations of the weld pool solidification [17] *etc.* are also frequently used to study solidification phenomena. None of the studies, however, have reported direct observation of liquid flow during the terminal stages of solidification.

In this work, solidification of a dual phase steel was observed *in-situ* using high temperature laser scanning confocal microscopy. This technique is frequently used to study *in-situ* solidification events like peritectic transformations and solid-state transformations, details of which can be found in the literature [18, 19]. In the present work, a circular melt pool was formed at the centre of a thin circular disk specimen while the outer rim remained solid. The solid outer rim acted as a restraint to the solidifying melt pool, thus allowing the simulation of welding conditions. During the terminal stages of solidification, liquid feeding was observed in inter-cellular regions. The feeding rate in these regions is calculated and subsequently the pressure that causes liquid feeding is estimated.

A commercial dual phase steel sheet with a composition, C 0.15, Mn 2.3, Cr 0.56, Si 0.1, Al 0.03, P 0.01 (all in wt. %) was examined in this study. Circular disk specimens with a diameter of 10 mm and a thickness between 200 µm - 250 µm were prepared using electro-discharge machining. Each specimen was placed in an alumina crucible. To minimise direct contact with the alumina crucible, the sample was held by ceramic protrusions at the circumference of the crucible. The crucible in turn was held in a platinum holder. A B-type thermocouple wire was welded to the platinum holder. Specimens were placed at the upper focal point of a gold plated ellipsoidal cavity in an infra-red furnace beneath a quartz view port under an ultra-high purity inert gas atmosphere, >99.9999% Ar. A 1.5 kW halogen lamp located at the lower focal point in the cavity heats the specimen by radiation. The power input to the halogen lamp is controlled by an Omron ES100P digital PID controller, which in turn was connected to the thermocouple at the crucible holder for a feedback signal. The temperature measured by the thermocouple incorporated in the crucible

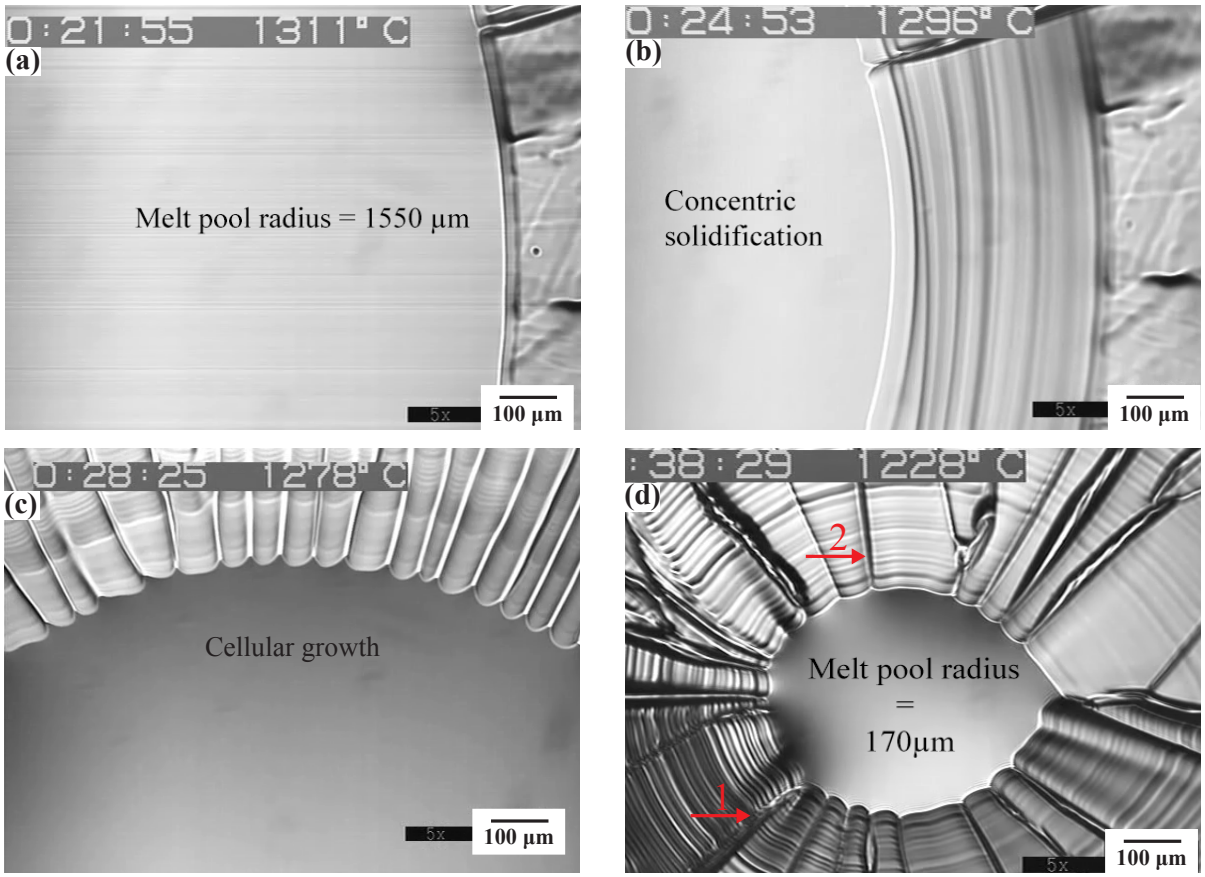

Fig. 1: Solidification images. (a) A stable melt pool of radius 1550 µm is formed to begin with. Afterwards a constant cooling rate of 5 K min^{-1} is applied, (b) solidification progresses in a concentric manner, (c) planar growth changes to cellular, (d) melt pool of radius 170 µm when liquid feeding in the inter-cellular regions was observed. Temperature indicated in images (a-d) is measured at the periphery of the platinum holder. Based on calibration the actual temperature is ~ 210 K higher.

holder was recorded while simultaneously, optical images were recorded at a rate of 30 frames per second. A stable melt pool with a diameter between 3-3.5 mm was obtained at the centre of the specimen while the outer rim remained solid. A cooling rate of 5 K min^{-1} was employed until 1623 K. To obtain an approximation of the actual temperature in the liquid pool, experiments with pure iron samples were conducted and a difference of 210 K was found between the thermocouple reading and melting point of iron (taken as 1811 K).

Fig. 1 shows the solidification sequence of the steel. A stable melt pool of diameter 3.1 mm was created before the cooling cycle started, as seen in Fig. 1 (a). Due to the slow cooling rate, the solidification front was initially observed to remain planar (Fig. 1 (b)). On further cooling, the interface morphology changed from planar to cellular growth as seen in Fig. 1 (c). On a macro scale, the solid/liquid interface was observed to propagate in a concentric manner throughout the solidification process. Concentric propagation of the interface was tracked using automatic video processing software for *in situ* interface tracking [20]. The radius of curvature of the interface can be used to calculate the fraction of solid and liquid at any time ~~(assuming solid and liquid to have~~

equal density). Fig. 1 (d) shows the terminal stage of the solidification during which the liquid feeding was observed in the inter-cellular regions. The fraction of liquid remaining was ≈ 1.2 % when compared to the original melt pool size. Two regions where liquid feeding was observed are marked in Fig. 1 (d) and further shown in Fig. 2 and Fig. 3 respectively. The liquid source for the feeding is the liquid remaining during the final stage of solidification in the centre. The process was dynamic and occurred in a matter of a few seconds. For better visualisation of the liquid flow, the reader can refer to the video file included as a supplement in the online version of this article. Fig. 2 shows the images from region 1 with F-n indicating the frame numbers. Time difference between successive frames is 33.33 ms. In order to determine the extent of liquid flow, reference gray scale image, Fig. 2 (a), was subtracted from subsequent images and resulting bitmap images show the extent of the liquid flow in the intervening time period. The pixels with no difference were then assigned a grey colour and the pixels where motion was detected were assigned a red colour; the results are shown in Fig. 2 (e)-(g). A similar procedure was followed for the region 2 and the results can be seen in Fig. 3. In our previous work [21], we performed high temperature confocal microscopy experiments on steels that are susceptible to cracking during laser welding [22]. Liquid feeding was not observed during solidification. Instead, solidification cracking was observed *in-situ* during the final stages of solidification.

Feurer [9] defined the maximum volumetric flow rate per unit volume (rate of liquid feeding, ROF) during solidification as:

$$ROF = \frac{\partial V}{V}.\frac{1}{\partial t} = \frac{\partial \ln V}{\partial t} = \frac{f_l^2 d^2 P_s}{24\pi c^3 \mu L^2}, \tag{1}$$

Here, f_l is the fraction of liquid, d is the secondary dendrite arm spacing, P_s is the effective feeding pressure, c is the tortuosity factor of the dendritic network, μ is the viscosity of the liquid phase and L is the length of the mushy zone. However, this equation is valid only in the case of dendritic solidification. In the current work, cellular growth was observed and the rate of liquid feeding applicable in this situation can be defined with the help of schematic presentation in Fig. 4. The solidification direction is assumed to be parallel to the "x" direction (Cartesian coordinate system) and the liquid also flows in the $-x$ direction. Rate of liquid feeding can be defined as:

$$ROF = \frac{\partial V}{V}.\frac{1}{\partial t} = \frac{v_{l,x}}{A}.\frac{A}{L} = \frac{v_{l,x}}{L}, \tag{2}$$

Where, $v_{l,x}$ is the unidirectional flow speed of liquid in the $-x$ direction, A is the cross-sectional area perpendicular to the growth direction and L is the length of the mushy zone. Due to a low solidification rate (0.75 µm s^{-1}), the cross-sectional area A is assumed to remain constant during the time period in which liquid flow was observed ($\Delta t = 0.3 - 0.4$ s).

The rate of solidification shrinkage (ROS) is given by:

$$ROS = \frac{\partial V}{V}.\frac{1}{\partial t} = -\frac{1}{\rho}.\frac{\partial \rho}{\partial t} = \frac{\beta}{\beta.f_s + 1}.\frac{\mathrm{d}f_s}{\mathrm{d}t}, \tag{3a}$$

with

$$\beta = \frac{\rho_\gamma - \rho_l}{\rho_l}, \tag{3b}$$

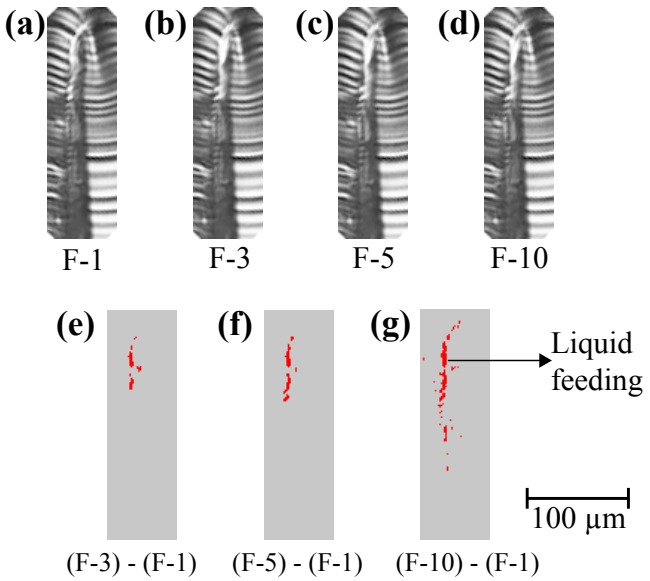

Fig. 2: Solidification images. Liquid flow observed in the inter-cellular region 1 as defined in Fig. 1(d). (a) is taken as the reference image, (b) liquid flow was observed, (c) and (d) liquid flow continues and reaches the bottom of the image when compared to the reference image, (e), (f) and (g) shows the extent of the liquid flow in images (b), (c) and (d) when compared to reference image (a). This was done using a MATLAB code to detect motion in a series of otherwise still images.

Where, f_s, f_l are the fractions of the solid and liquid, ρ_γ, ρ_l the densities of the austenite and liquid phases respectively. The rate of change of f_s can be calculated by determining f_s at various times during the course of solidification. Shrinkage factor of the steel was calculated as 3.8% using a commercial thermodynamic software Thermo-Calc^{TM}. The rate of solidification shrinkage is found to be $\approx 4.2 \times 10^{-6} s^{-1}$ during the period where liquid feeding was observed.

The rate of deformation (ROD) of the mushy region can be approximated as [23]:

$$ROD = -\alpha.\dot{T}, \tag{4}$$

Here, α is the linear thermal expansion coefficient when $f_s \approx 99$ %. $\dot{T}$ is the cooling rate. Assuming $\alpha = 1.2\,\mathrm{x10^{-5}K^{-1}}$ [24], the rate of deformation is $\approx 1\,\mathrm{x10^{-6}s^{-1}}$. In the current case, the rate of solidification shrinkage and the rate of deformation are found to be of the same order. To avoid the formation of voids which can later lead to solidification cracking, the rate of liquid feeding should be higher than both rate of solidification shrinkage and rate of deformation combined.

The average velocity of the liquid ($v_{l,x}$) in the inter-cellular channel was calculated by image analysis and was found to be $450\,\mu\mathrm{m\,s^{-1}}$ and $500\,\mu\mathrm{m\,s^{-1}}$ in regions 1 and 2 respectively. Such high velocities can exist due to a pressure drop in the cavities between the cells. The length of the mushy zone was 250 µm. The rate of liquid feeding ($\approx 2\,\mathrm{s^{-1}}$) calculated from equation (2) is six orders of magnitude higher than the rate of solidification shrinkage and the rate of deformation combined. As a result, no solidification cracking is expected and indeed no crack was observed during solidification. The velocity of the liquid in the mushy zone is related to the pressure gradient in the liquid via the Darcy's equation [10, 25],

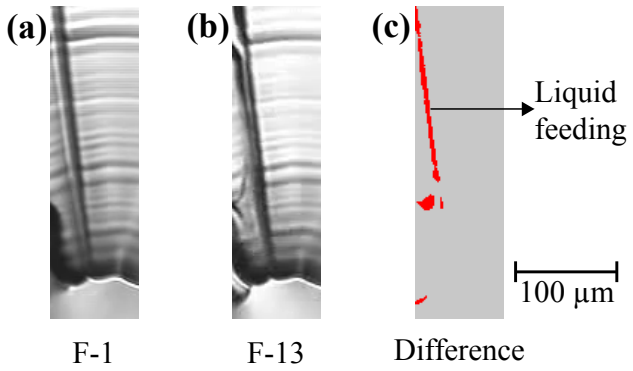

Fig. 3: Solidification images. Liquid flow observed in the inter-cellular region 2 as defined in Fig. 1(d). (a) is taken as the reference image , (b) liquid flow observed, (c) shows the extent of liquid feeding.

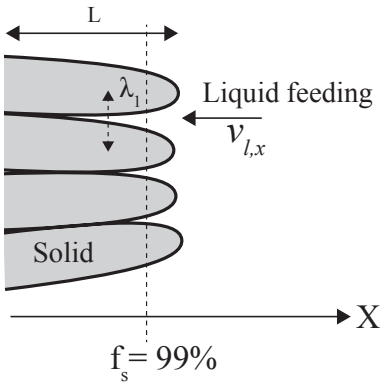

Fig. 4: Schematic illustration of the liquid feeding observed in the experiments. Rate of feeding criterion applied for cellular growth.

$$v_{l,x} f_l = -\frac{K}{\mu}\frac{\Delta P}{L}, \tag{5}$$

Where $v_{l,x}$ is the velocity of the liquid, f_l is the fraction of liquid, K is the permeability in the mushy zone and μ is the viscosity of the liquid. The contribution of gravity has been neglected in this equation. Permeability data is scarce for $f_l \leq 0.17$. For extrapolations, Poirier recommended the use of models based on Blake-Kozeny equations [26]. The permeability defined by the Blake-Kozeny relationship [26] is given by,

$$K = C_2 \frac{\lambda_1^2 f_l^3}{(1 - f_l)}, \tag{6a}$$

with

$$C_2 = 4.53 \times 10^{-4} + 4.02 \times 10^{-6}(f_l + 0.1)^{-5}, \tag{6b}$$

Where, λ_1 is the inter-cellular spacing and f_l is the fraction of liquid. C_2 was obtained by regression analysis. The average spacing was = 45 $\pm 10 \mu m$. Using the fraction of liquid (f_l) = 0.01, the value of permeability in the mushy region was calculated as $6.3 \times 10^{-16} m^2$. The value

is reasonable since for a Pb - 20 wt. % Sn alloy with primary dendrite arm spacing 51 μm and higher liquid fration (f_l = 0.19), Streat *et al.* [27] reported higher permeability values of the order of $10^{-14} m^2$.

Considering the fluid behaviour to be Newtonian, the dynamic viscosity (μ) was assumed to be constant as 4.9 mPa s [28]. Moreover, the temperature change during which the flow occurred was found to be negligible (cooling rate $\approx 0.083\,\mathrm{K\,s^{-1}}$). The pressure difference was then calculated from Darcy's equation (5) and an average pressure difference (in regions 1 and 2) of the order of 10^4 Pa is found. To the best knowledge of authors, this is the first time that an experimentally derived feeding pressure has been reported. While mentioning it as an unknown key value, Rappaz *et al.* [10] assumed a cavitation pressure value of 2 kPa for Al - 1.4 wt. Cu % alloy in their study. The higher magnitude in this steel compared to Al-alloys can be attributed to higher cracking susceptibility of Al-alloys owing to the large solidification shrinkage contribution (solid, liquid density difference $\sim$ 6-8 %) [29]. Furthermore, Eskin *et al.* [30] reported higher linear thermal expansion coefficient of Al - Cu (1 - 5 wt. %) alloys in the range of (2.8 - 3) $\times\ 10^{-5}\,\mathrm{K^{-1}}$. No hot tearing or solidification cracking occurred during solidification of the steel in the present case, therefore the cavitation pressure for this steel must exceed 10^4 Pa. Higher cavitation pressure is required in order to form a cavity due to the lack of liquid feeding.

In summary, solidification of a dual phase steel was observed *in-situ* under a high temperature laser scanning confocal microscope. Liquid feeding occurred during the terminal stage of solidification in the inter-cellular regions. Liquid flow speed in the inter-cellular regions was derived and the pressure difference that causes liquid flow was estimated by means of Darcy's equation. It was also found that rate of liquid feeding was higher than the rate of solidification shrinkage and rate of deformation, combined.

Acknowledgements

This research was carried out under project number F22.8.13485a in the framework of the Partnership Program of the Materials innovation institute M2i (www.m2i.nl) and the Foundation for Fundamental Research on Matter (FOM) (www.fom.nl), which is part of the Netherlands Organisation for Scientific Research (www.nwo.nl). The authors would like to thank the industrial partner in this project 'Tata Steel Nederland B.V.' for the financial support. Professor Laurens Katgerman is acknowledged for useful discussion.

[1] S. Kou, Acta Mater. 88 (2015) 366–374.
[2] L. Aucott, D. Huang, H. Dong, S. Wen, J. Marsden, A. Rack, A. Cocks, Sci. Rep. 7 (2017).
[3] S. A. David, T. DebRoy, Science 257 (1992) 497–502.
[4] W. S. Pellini, Foundry 80 (1952) 124–133.
[5] N. N. Prokhorov, Svar Proiz 6 (1956) 5–11.
[6] I. Medovar, Avtomatich. Svarka 7 (1954) 12–28.
[7] C. E. Cross, in: T. Böllinghaus, H. Herold (Eds.), Hot Cracking Phenomena in Welds, Springer Berlin Heidelberg, 2005, pp. 3–18.
[8] D. G. Eskin, L. Katgerman, Metall. Mater. Trans. A 38 (2007) 1511–1519.
[9] U. Feurer, Proceedings of the international symposium on engineering alloys, Delft (1977) 131–145.
[10] M. Rappaz, J.-M. Drezet, M. Gremaud, Metall. Mater. Trans. A 30 (1999) 449–455.
[11] H. Yasuda, I. Ohnaka, K. Kawasaki, A. Sugiyama, T. Ohmichi, J. Iwane, K. Umetani, J. Cryst. Growth 262 (2004) 645 – 652.

[12] N. Iqbal, N. van Dijk, S. Offerman, M. Moret, L. Katgerman, G. Kearley, Acta Mater. 53 (2005) 2875 – 2880.
[13] P. Schaffer, R. Mathiesen, L. Arnberg, Acta Mater. 57 (2009) 2887 – 2895.
[14] R. Mathiesen, L. Arnberg, F. Mo, T. Weitkamp, A. Snigirev, Phys. Rev. Lett. 83 (1999) 5062–5065.
[15] T. Nagira, C. Gourlay, A. Sugiyama, M. Uesugi, Y. Kanzawa, M. Yoshiya, K. Uesugi, K. Umetani, H. Yasuda, Scr. Mater. 64 (2011) 1129 – 1132.
[16] M. Vandyoussefi, H. Kerr, W. Kurz, Acta Mater. 48 (2000) 2297–2306.
[17] P. von Witzendorff, S. Kaierle, O. Suttmann, L. Overmeyer, Metall. Mater. Trans. A 46 (2015) 1678–1688.
[18] H. Shibata, Y. Arai, M. Suzuki, T. Emi, Metall. Mater. Trans. B 31 (2000) 981–991.
[19] M. Reid, D. Phelan, R. Dippenaar, ISIJ Int. 44 (2004) 565–572.
[20] S. Griesser, R. Pierer, M. Reid, R. Dippenaar, J. Microsc. 248 (2012) 42–48.
[21] G. Agarwal, M. Amirthalingam, M. J. M. Hermans, I. M. Richardson, S. C. Moon, R. J. Dippenaar, in: The International Symposium on Visualization in Joining and Welding Science through Advanced Measurements and Simulation, volume 1, Joining and Welding Research Institute, Osaka University, pp. 113–114.
[22] H. Gao, G. Agarwal, M. Amirthalingam, M. J. M. Hermans, Sci. Technol. Weld. Join. 0 (2017) 1–8.
[23] M. Drezet, M. S. F. Lima, J. D. Wagniere, M. Rappaz, W. Kurz, in: P. Mayr, G. Posch, H. Cerjak (Eds.), Proc. of the International Institute of Welding Conference, pp. 87–94.
[24] X. Li, L. Wang, L. Yang, J. Wang, K. Li, J. Mater. Process. Technol. 214 (2014) 1844 – 1851.
[25] K. Kubo, R. D. Pehlke, Metall. Trans. B 16 (1985) 359–366.
[26] D. R. Poirier, Metall. Trans. B 18 (1987) 245–255.
[27] N. Streat, F. Weinberg, Metall. Trans. B 7 (1976) 417–423.
[28] J. H. Hildebrand, R. H. Lamoreaux, Proc. Natl. Acad. Sci. U.S.A. 73 (1976) 988–989.
[29] D. G. Eskin, Physical Metallurgy of Direct Chill Casting of Aluminum Alloys, CRC Press, 2008.
[30] D. G. Eskin, L. Katgerman, Suyitno, J. F. Mooney, Metall. Mater. Trans. A 35 (2004) 1325–1335.